Nanoscale

ROYAL SOCIETY OF CHEMISTRY

COMMUNICATION

View Article Online
View Journal



Cite this: DOI: 10.1039/c9nr08060k

Received 18th September 2019,
Accepted 10th February 2020

DOI: 10.1039/c9nr08060k

rsc.li/nanoscale

# Photon induced quantum yield regeneration of cap-exchanged CdSe/CdS quantum rods for ratiometric biosensing and cellular imaging†

Weili Wang, ‡[a] Yifei Kong,‡[a] Jun Jiang,[b] Xin Tian,[b] Shuang Li,[c] Uchangi Satyaprasad Akshath,[a] Christian Tiede,[d] Nicole Hondow,[e] Anchi Yu,[c] Yuan Guo *[f] and Dejian Zhou *[a]

**Full water-dispersion of commercial hydrophobic CdSe/CdS core/shell quantum rods (QRs) was achieved by cap-exchange using a dihydrolipoic acid zwitterion ligand at a low ligand:QR molar ratio (LQMR) of 1000. However, this process almost completely quenched the QR fluorescence, greatly limiting its potential in downstream fluorescence based applications. Fortunately, we found that the QR fluorescence could be recovered by exposure to near ultra-violet to blue light radiation (*e.g.* 300–450 nm). These "reborn" QRs were found to be compact, bright, and stable, and were resistant to non-specific adsorption, which make them powerful fluorescent probes in broad biomedical applications. We demonstrated their potential in two model applications: first, the QRs were conjugated with $His_8$-tagged small antibody mimetic proteins (also known as Affimers) for the sensitive detection of target proteins *via* a Förster resonance energy transfer (FRET) readout strategy and second, the QR surface was functionalized with biotins for targeted imaging of cancer cells.**



## 1. Introduction

Over the past three decades, fluorescent semiconductor nanocrystals (*aka* quantum dots, QDs) have been a major research focus owing to their unique size-dependent, bright, and stable fluorescence which makes them powerful fluorescent probes in broad biomedical applications.[1–6] Compared to spherical QDs, elongated rod-shaped quantum rods (QRs) have a higher extinction coefficient and single particle brightness, making them potentially more powerful fluorescent probes.[7–10] Moreover, their photophysical properties can be further tuned by altering the aspect (length/width) ratio, which can be extremely beneficial for certain biomedical applications. For example, the aspect ratio has been found to strongly affect the bioluminescence resonance energy transfer (BRET) between a CdSe/CdS core/shell QR and self-assembled firefly luciferase, and an aspect ratio of ~3 gives the highest BRET ratio.[9]

To date, most high-quality QRs have been synthesised using organometallic precursors in high boiling point coordinating solvents, through which their size and aspect ratio can be finely controlled.[7,10] These QRs are naturally capped with hydrophobic ligands, making them only dispersible in non-polar organic solvents and hence are biologically incompatible. As a result, they must be made water-dispersible and biocompatible prior to any biomedical applications. In this regard, amphiphilic polymer encapsulation or coating with silica shells has been widely employed.[1–3,7] Despite their success, these methods typically yield relatively bulky QRs (with hydrodynamic diameter, $D_h$ > 20 nm) which can limit their applications in conditions that require compact sizes, *e.g.* imaging of crowded neuronal synapse, and particularly, in Förster resonance energy transfer (FRET) based applications.[4–6,12–17] This is because of the inverse 6$^{th}$ power dependence of the FRET efficiency ($E$) with a donor–acceptor distance ($r$), $E = 1/[1 + (r/R_0)^6]$, where $R_0$ is the Förster radius of the FRET pair and $r$ is the average QR–dye distance. To improve $E$, it is important to reduce $r$ to a reasonable range (*e.g.* comparable to $R_0$). Accordingly, cap-exchange is better suited here because it can produce compact sizes required to achieve a high FRET efficiency. In this regard, cap-exchange using poly (ethylene glycol) (PEG) or zwitterionic based ligands appending the dihydrolipoic acid (DHLA)-, poly-DHLA- or poly-histidine-based multi-dentate anchoring group has successfully transferred hydrophobic core/shell QDs into hydrophilic ones. The resulting QDs have been widely used in biosensing, bioimaging, cell tracking, and super-resolution imaging applications.[14–21]

[a]School of Chemistry and Astbury Centre for Structural Molecular Biology, University of Leeds, Leeds LS2 9JT, UK. E-mail: d.zhou@leeds.ac.uk
[b]School of Biology & Basic Medical Sciences, Soochow University, Suzhou 215100, People's Republic of China
[c]Department of Chemistry, Renmin University of China, Beijing 100872, People's Republic of China
[d]School of Molecular and Cellular Biology and Astbury Centre for Structural Molecular Biology, University of Leeds, Leeds LS2 9JT, UK
[e]School of Chemical and Process Engineering, University of Leeds, Leeds LS2 9JT, UK
[f]School of Food Science and Nutrition and Astbury Centre for Structural Molecular Biology, University of Leeds, Leeds LS2 9JT, UK. E-mail: y.guo@leeds.ac.uk

†Electronic supplementary information (ESI) available. See DOI: 10.1039/c9nr08060k

‡Equal contribution.

Despite their success, these strongly chelating ligands have rarely been applied in CdSe/CdS QRs, the most widely studied QRs. In addition, a common drawback of cap-exchange using such strong chelating ligands has been a significant decrease in the fluorescence quantum yield (QY) of the cap-exchanged QDs, limiting their potential as fluorescent probes. Although this problem can be addressed by growing a thick inorganic shell to insulate the fluorescent core from the outer environment, making them more resilient to environmental changes caused by cap-exchange,[22] it is not applicable for most commercial core/shell QDs which are known to have relatively thin shells. Moreover, growing a thick shell can significantly increase the overall QD size, leading to reduced FRET efficiency. Recently, we have found that shell etching during cap-exchange is a major factor responsible for the quenched fluorescence of commercial CdSe/ZnS QDs.[12] By fully deprotonating the DHLA thiol groups to enhance the cap-exchange efficiency and reducing the ligand : QD molar ratio (LQMR) to the minimum, just sufficient to promote full QD cap-exchange and form isolated single QD dispersions, to minimise any possible shell etching, we have unveiled an ultra-efficient cap-exchange protocol which has successfully transferred the commercial hydrophobic CdSe/ZnS and CdSe/ZnSe/ZnS QDs into stable, compact, and water-dispersible ones while retaining >90% of their original fluorescence.[12]

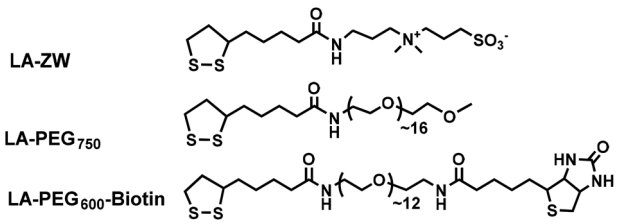


**Scheme 1** Chemical structures and their abbreviations of the ligands employed in this study.

Here we extended this efficient cap-exchange method to commercial hydrophobic CdSe/CdS core/shell QRs (consisting of a CdSe dot in a CdS rod structure of approximately 3.6 nm width and 24 nm length as revealed by TEM imaging, see the ESI, Fig. S1†) with DHLA-based ligands. Similar to the CdSe/ZnS QDs reported previously, stable QR water-dispersions were readily prepared at a low LQMR of 1000. However, to our surprise, the cap-exchanged QRs were found to be almost fully quenched, making them unusable as fluorescent probes. Fortunately, we discovered that the fluorescence of the QR could be recovered slowly upon exposure to ambient room light and this photon activation process was accelerated by exposing to stronger lights in the near UV to visible region of the spectrum, with the light wavelength ($\lambda$) of 350–450 nm being optimal. Moreover, the fluorescence regenerated QRs were readily functionalised with Affimers (small antibody mimetic proteins)[23] for FRET based ratiometric biosensing or biotins for targeted imaging of cancer cells.

## 2. Results and discussion

### 2.1. QR water-dispersion and characterisation

Scheme 1 shows the chemical structures of the lipoic acid (LA)-based ligands appending different terminal functional groups (*e.g.* zwitterion, $PEG_{750}$, and $PEG_{600}$-biotin) used in this study. These ligands were synthesized by following the literature procedures and purified by either column chromatography (for LA-$PEG_{750}$ and LA-$PEG_{600}$-biotin) or by high performance liquid chromatography (for LA-zwitterion).[12,15] Details of the ligand synthesis procedures and their spectroscopic data were reported previously.[12]

The procedures to transfer hydrophobic QRs into water-dispersed ones and the corresponding photographs following each step are shown in Fig. 1A/B. The cap-exchange conditions were optimised by performing cap-exchange under different

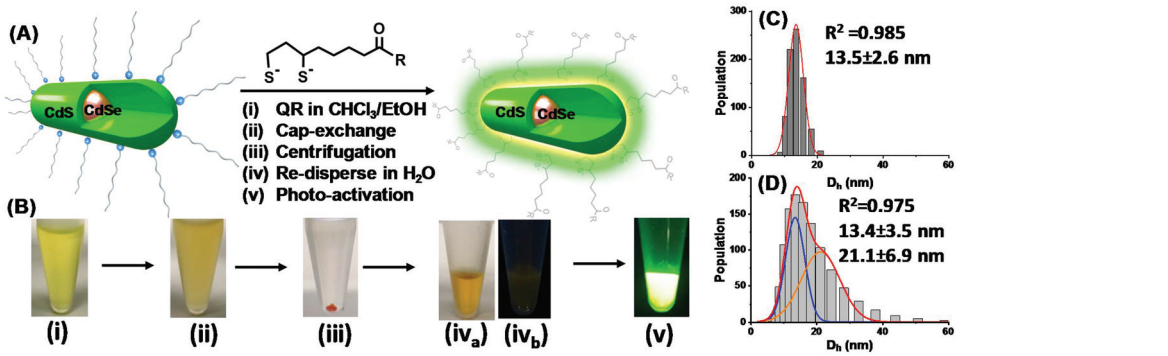


**Fig. 1** (A) Schematic showing the steps involved in transferring hydrophobic QRs into water-dispersed ones by cap-exchange using DHLA-ZW and photon activation. (B) Photographs showing (i) a CdSe/CdS QR ($\lambda_{EM}$ ~ 550 nm) dispersed in a mixed $CHCl_3$/EtOH solvent, (ii) after mixing with the deprotonated DHLA-ZW ligand, (iii) after centrifugation; (iv) after removal of the supernatant and dispersion in $H_2O$ under ambient- ($iv_a$) or UV- ($iv_b$) light illumination, (v) after exposure to 4 h UV light treatment of a TLC UV-lamp ($\lambda$ = 365 nm) under UV light illumination. (C) Hydrodynamic diameter ($D_h$) histograms and Gaussian fitting of a freshly prepared DHLA-ZW capped QR showing a single species of 13.5 ± 2.6 nm (mean ± ½ FWHW, full width at half maximum). (D) The $D_h$ histograms of the QR after 4 h UV light ($\lambda$ = 365 nm) activation showing two Gaussian species of 13.4 ± 3.5 (~43% area, blue line) and 21.1 ± 6.9 nm (~57% area, orange line), respectively.

LQMRs and monitoring the QR water-dispersion ability and hydrodynamic diameter ($D_h$), ensuring that a full water-dispersion and small $D_h$ were obtained.[12] The optimised procedures with 0.2 nmol QRs were as follows. First, commercial CdSe/CdS QR stock (20 μM stock, 10 μL in hexane) was precipitated by adding 500 μL of EtOH followed by centrifugation to remove any unbound free ligands. The QR pellet was dissolved in 100 μL $CHCl_3$ and then 50 μL EtOH was added to make a uniform solution (Fig. 1B(i)). Meanwhile, the LA-ZW ligand (0.10 M, 2 μL in $H_2O$) was reduced to DHLA-ZW by mixing with 1 molar equivalent of tris(2-carboxyethyl)phosphine hydrochloride (TCEP·HCl, 0.10 M, 2 μL in $H_2O$) for 15 min. The reduction of LA to DHLA by TECP was rapid and quantitative as reported previously.[24] It could be readily visualised by the naked eye by the disappearance of the yellow colour (due to absorption of LA thiolane). After this, NaOH (0.10 M in EtOH, 12 μL, NaOH : DHLA-ZW ligand molar ratio = 6 : 1) was added to fully deprotonate DHLA di-thiol groups and to neutralise TCEP·HCl's four acid groups. The resulting solution was then added to the QR dispersion above and thoroughly mixed by shaking by hand for ~1 min. The solution became turbid quickly, indicating the formation of DHLA-ZW capped QRs which had very low solubility in a mixed $CHCl_3$/EtOH solvent (Fig. 1B(ii)). The suspension was centrifuged (3000 rpm for 10 s) and the QR was pelleted at the bottom of the tube, leaving the supernatant colourless (Fig. 1B(iii)). After careful removal of the supernatant, the QR pellet was dispersed in $H_2O$ (100 μL) to give a clear, stable solution (Fig. 1B($iv_a$). The freshly prepared QRs were effectively non-emissive (Fig. 1B($iv_b$), but were readily transformed into brightly fluorescent ones after 4 h photon activation using a thin layer chromatography (TLC) UV lamp ($\lambda$ = 365 nm, Fig. 1B(v)). The QR concentration was determined from its 1$^{st}$ exciton peak absorption at ~545 nm using an extinction coefficient of $2.56 \times 10^5$ $M^{-1}$ $cm^{-1}$.[17]

The QR water-dispersion prepared with the DHLA-ZW ligand at a LQMR of 1000 (abbreviated as QR-ZW hereafter) was stable and showed no sign of precipitation or changes in the physical appearance after storage for at least 3 months in darkness (wrapped in aluminium foil). Its $D_h$ sizes measured by dynamic light scattering showed a narrow size distribution which was fitted well by the Gaussian function ($R^2$ = 0.985), giving a single $D_h$ species of 13.5 ± 2.6 nm (mean ± $\frac{1}{2}$ FWHM, FWHM = full width at half maximum obtained from Gaussian fitting, Fig. 1C).[12] Despite not being spherical in shape, the QR's diffusion coefficient was comparable to that of a sphere of ~13.5 nm, a value that lay in between the width and length of the QR, and was ~1/2 that of the QR length after taking the DHLA-ZW ligand coating thickness into consideration. This indicated that the QR-ZW obtained here was made of isolated single QR particles, and not aggregated/clustered ones.

Theoretically, a cylinder shaped QR of 3.6 nm width and 24 nm length would have a total surface area of 291 $nm^2$. Assuming that CdS adopted its stable wurtzite structure and terminated with a full $Cd^{2+}$ outer layer, then each QR would have 1940 $Cd^{2+}$ ions on its surface (see the ESI, Fig. S2†). Assuming that each thiolate coordinated to one $Cd^{2+}$ ion, a LQMR of 970 with the DHLA-based ligand (each having 2 thiol groups) would completely cap all the QR surface $Cd^{2+}$ ions and form a stable water-dispersion. This number matched well with the observation that a LQMR of 1000 was able to completely water-disperse the QR and form isolated single particles. Significantly, the LQMR used here to achieve complete QR water-dispersion was 1–2 orders of magnitude lower than that used in most literature methods,[11,14–21] suggesting the ultra-efficiency of our cap-exchange method. Moreover, this calculation also indicated that there should be almost no free DHLA-ligands left in the system to produce any photo-chemical transformations.[25] Nonetheless, this result was fully consistent with those obtained with the CdSe/ZnS and CdSe/ZnSe/ZnS QDs reported previously.[12] Moreover, a TEM image of the cap-exchanged QRs revealed that they had almost identical particle shapes and sizes to the parent QRs prior to cap-exchange (ESI, Fig. S1†), suggesting no observable etching of the QR structure after cap-exchange. This result was also consistent with our above estimation that most of the added DHLA-ZW ligands should have capped onto the QR surface, leaving almost no free ligands that could etch the QR shell surface $Cd^{2+}$ ions.[12]

### 2.2. Photon-induced QR fluorescence regeneration

Despite its success in promoting full QR water-dispersion, the resulting QR-ZW was found to be almost completely quenched, retaining just ~2% of its original fluorescence (in $CHCl_3$). In contrast, the CdSe/ZnS and CdSe/ZnSe/ZnS[12] QDs were able to retain >90% of their original fluorescence under equivalent cap-exchange conditions (see the ESI, Fig. S3†).[12] The difference here was likely due to the different band energy levels of the core and shell structures. Both the CdSe/ZnS and CdSe/CdS/ZnS QDs had a type-I core/shell band structure whose exciton carriers (electron and hole) were fully confined within the core,[26] and thus a small change to the shell induced by cap-exchange would not significantly affect their fluorescence (see the ESI, Fig. S4†). However, the CdSe/CdS QR had a Quasi-type II core/shell band structure: the hole was confined in the core, but the electron was spread across both the core and shell structure.[26] As a result, the QR is much more sensitive to even small changes to the shell: any new surface defects induced by cap-exchange could trap the excited electron and prevent its emissive recombination with the hole, giving rise to greatly quenched QR fluorescence.[26] This problem greatly limited the potential use of the CdSe/CdS QRs as fluorescent probes in biomedical research. Moreover, this problem could not be solved by reducing the LQMR to the minimum (*e.g.* 1000 here) to minimize shell etching as we had achieved successfully with the type I QDs.[12] Fortunately, we discovered that the fluorescence of the QRs gradually recovered over a few weeks upon exposure to ambient room light during storage, and the recovery rate was increased by exposing to UV light ($\lambda$ = 365 nm, see the ESI, Fig. S5†).

To investigate the driving force of this photon induced fluorescence regeneration, a freshly prepared QR-ZW was divided into 3 portions and exposed to different light conditions: UV

light (a TLC UV lamp, $\lambda$ = 365 nm), ambient room light, or in darkness (wrapped in aluminum foil). The QR exposed to UV light was found to recover rapidly, regaining ~82% of its original fluorescence in 5 h (Fig. S5A†). The QR exposed to ambient room light recovered slowly, regaining ~62% of its original fluorescence over 1 week (Fig. S5B†). The QR stored in darkness with occasional exposure to ambient room light (when taken out for inspection) showed very slow fluorescence recovery over 4 weeks (Fig. S5C†). This result revealed that both the intensity and wavelength of light radiation played an important role in the QR fluorescence recovery. Moreover, the photon activation behavior appeared to be general and applicable to other DHLA-based ligand capped QRs. For example, an initially "dark" DHLA-$PEG_{750}$ capped QR showed greatly enhanced fluorescence after 4 h UV light activation ($\lambda$ = 365 nm, *via* a TLC UV lamp), similar to that observed with QD-ZW. Moreover, it could retain the bright fluorescence for at least 1 month (see the ESI, Fig. S6†), suggesting that the photon activation effect was permanent.

To further investigate the dependence of QR fluorescence recovery on the wavelength of the exposing light, a freshly prepared QR-ZW water-dispersion (a different batch, $\lambda_{EM}$ = ~570 nm) was placed in a cuvette and its emission spectrum was repeatedly recorded using a fluorometer under a given excitation wavelength (*e.g.* $\lambda_{EX}$ = 200, 300, 350, 400, 450 or 500 nm, respectively). The resulting scan number dependent fluorescence spectra revealed that QR fluorescence regeneration was only observed with $\lambda_{EX}$ over a range of 300–450 nm, but not at a longer (*e.g.* 500 nm) or shorter (*e.g.* 200 nm) wavelength (see Fig. 2). In the longer $\lambda_{EX}$ range, it appeared that the QR fluorescence could only be regenerated with photon energy higher than the $1P_{3/2} \rightarrow 1P_e$ transition ($\lambda$ = ~460 nm as measured by transient absorption, see the next section). Interestingly, the photon activation process typically displayed three different stages. First, a lag phase where a minimal fluorescence increase was observed with an increase in the number of scans, followed by a photon activation phase where the QR fluorescence increased rapidly and roughly linearly with the number of scans, and finally a saturation phase where the QR fluorescence plateaued. $\lambda_{EX}$ = 400 nm was found to be optimal for QR fluorescence regeneration: it gave the smallest number of scans in the lag phase (~10 *vs.* ~18 or ~25 for $\lambda_{EX}$ = 350 or 450 nm, respectively) and the highest increase rate per scan at the photon activation phase (ESI, Table S1†). Overall, >16 fold fluorescence enhancement was achieved with this batch of QR-ZW *via* photon-activation (Fig. 2D). This result thus established a facile route to control the QR fluorescence regeneration by simply applying a certain number of emission scans under a certain $\lambda_{EX}$.

Interestingly, careful analysis of the fluorescence spectra during the repeated emission scans revealed a small but noticeable blue shift of the peak $\lambda_{EM}$ at ~6 nm (from ~570 to ~564 nm) with the photon regenerated QRs. Moreover, the onset of photon activation appeared to be coincident with the blue shift of the $\lambda_{EM}$. This result was consistent with the photo-oxidation induced fluorescence brightening mechanism previously observed with CdSe/CdS/ZnS QRs by the Alivisatos group[10a] and a CdSe/CdS QD by the Peng group.[10b] Moreover, the $D_h$ distribution histograms of a UV-light regenerated QR (4 h exposure with a TLC UV lamp, $\lambda$ = 365 nm) were best fitted

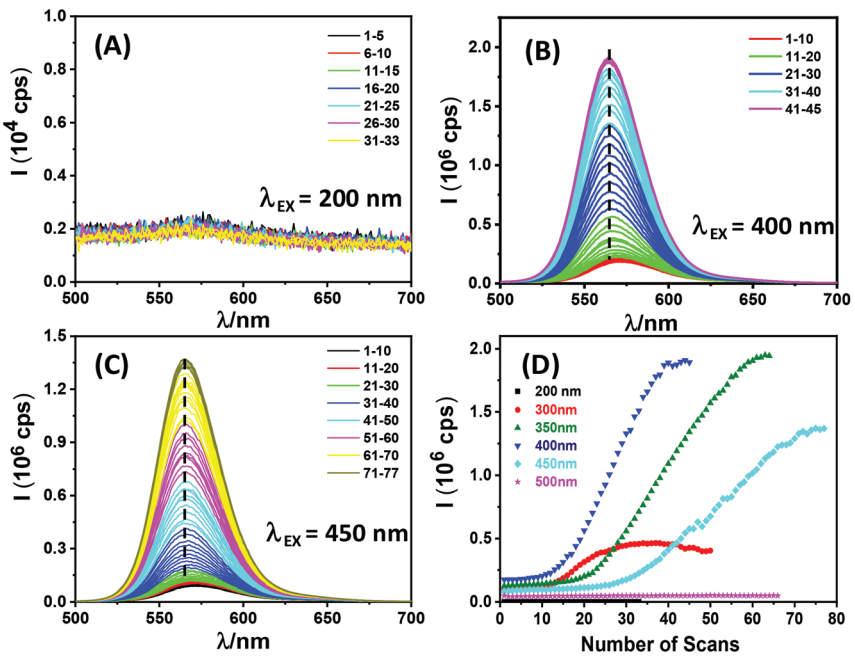


**Fig. 2** Fluorescence spectra of a freshly prepared DHLA-ZW ligand capped CdSe/CdS QR in $H_2O$ (5 nM) after repeated emission scans at a fixed excitation wavelength ($\lambda_{EX}$) of (A) 200 nm, (B) 400 nm and (C) 450 nm. (D) A plot of the QR fluorescence intensity *versus* the number of scans under different $\lambda_{EX}$.

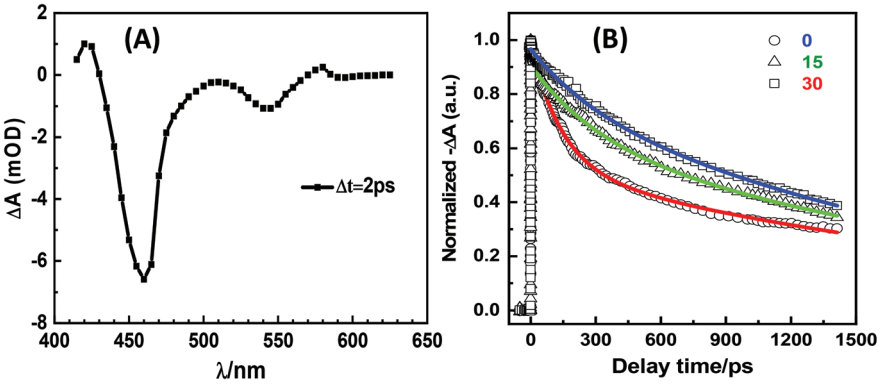


Fig. 3 (A) Femtosecond transient absorption spectrum of the 30 day ambient room light activated QR in $H_2O$ recorded at 2 ps after 460 nm excitation. (B) Decay kinetics of the QRs in $H_2O$ after different light treatment conditions: freshly prepared without photon activation (○), after exposure to ambient room light for 15 (△) or 30 (□) days. Pump wavelength: 460 nm; probe wavelength: 470 nm.

by two Gaussian species, giving $D_h$ values of 13.4 ± 0.3 (FWHM: 5.9 nm, 43% of area) and 21.1 ± 2.3 nm (FWHM: 11.8 nm, 57% of area), respectively (see Fig. 1D). The smaller species was almost identical to the freshly prepared QD-ZW particles, while the bigger ones could be assigned to clustered QRs after photon activation. Furthermore, prolonged exposure of the QRs to UV light radiation (*e.g.* >10 h, with a TLC UV lamp) produced extensive QR aggregation that eventually led to precipitation. This result was consistent with the reduced QR colloidal stability due to ligand depletion induced by photo-oxidation. All these results suggested that photo-oxidation induced fluorescence brightening[10] was the most likely mechanism behind the observed QR fluorescence regeneration here.

Importantly, the photon regenerated QRs (4 h UV light exposure) still exhibited a $D_h$ size useful for passive cancer tumour targeting *via* the enhanced permeation and retention (EPR) effect, a characteristic pathological condition of many cancer tumours.[27a] They were bigger than the gaps of healthy blood vessels (to reduce non-specific accumulation in healthy tissues) and the renal clearance threshold (~8 nm, to allow for prolonged blood circulation time),[27b] but were smaller than the average gaps of the leaky blood vessels in tumours (*e.g.* up to 200 nm) and so could easily diffuse into and accumulate inside tumours. A combination of bright fluorescence and suitable $D_h$ sizes for EPR based passive targeting made such QRs attractive for potential *in vivo* cancer tumour targeting and imaging applications.

To further investigate the mechanism of photon activation, we recorded the transient absorption spectra of a freshly prepared "dark" QR-ZW and two such QRs after photon activation *via* exposure to ambient room light for 15 and 30 days, respectively, on a femto-second transient absorption system.[28] The transient absorption spectra showed two apparent negative bands, a weak band at 545 nm (corresponding to the first excitonic transition of the CdSe core, $1S_{3/2} \rightarrow 1S_e$ and $2S_{3/2} \rightarrow 1S_e$) and a strong band at 460 nm (assigned to the $1P_{3/2} \rightarrow 1P_e$ transition, see Fig. 3A).[28,29] To better understand how photon activation affected the QR transient absorption, the time dependent decay curves at 470 nm were investigated. The decay curves of the freshly prepared "dark" QR could be fitted well by two exponential decays, while the photon regenerated QRs were best fitted by three exponential decays (Fig. 3B). The resulting fitting parameters are summarized in Table 1. The average lifetime ($\tau_{ave}$) of the QR was found to have increased considerably after photon activation, suggesting that photon activation reduced some rapid energy dispersion pathways (possibly due to the reduction of the QR surface electron traps *via* photon oxidation). Due to the short 1P to 1S relaxation lifetime, the lifetime from $1P_{3/2}$ to $1P_e$ approximated to the lifetime from $1S_{3/2}$ to $1S_e$.[28,29] This result was consistent with the steady-state fluorescence spectra observed above.

### 2.3. QR-Affimer for ratiometric biosensing

The high brightness of the photon regenerated QRs made them attractive for FRET-based sensing applications. To explore this potential, the QR-ZW was first photon regenerated by exposure to a TLC UV lamp ($\lambda$ = 365 nm) for 4 h. Affimers were selected as the target protein binders due to their small molecular sizes (<1/10 of a full antibody)[23] which could significantly reduce the FRET distance ($r$) and improve sensitivity.[12] Here an anti-yeast SUMO (small ubiquitin-like modifier)

Table 1 Fitting parameters of the kinetic curves of the DHLA-ZW ligand capped QR in $H_2O$ before and after photon activation. $\tau_{ave} = \tau_1 \times a_1 + \tau_2 \times a_2 + \tau_3 \times a_3$

| Sample | $a_1$ | $\tau_1$/ps | $a_2$ | $\tau_2$/ps | $a_3$ | $\tau_3$/ps | $\tau_{ave}$/ps |
|---|---|---|---|---|---|---|---|
| 0 | — | — | 0.46 | 145 ± 10 | 0.54 | 2330 ± 50 | 1320 ± 50 |
| 15 day | 0.09 | 3 ± 0.5 | 0.25 | 310 ± 10 | 0.66 | 2240 ± 50 | 1560 ± 50 |
| 30 day | 0.05 | 2 ± 0.5 | 0.57 | 770 ± 50 | 0.38 | 6400 ± 50 | 1650 ± 50 |

Affimer was used to detect the target SUMO protein, acting as a model disease biomarker.[23] The Affimer was modified by a C-terminal $His_8$-tag for convenient QR conjugation *via* a facile metal-affinity self-assembly process as reported previously.[4a,12,23]

First, we studied the QR-Affimer self-assembly by mixing an Atto-594 labeled Affimer with the QR-ZW ($\lambda_{EM}$ ~ 550 nm) under different molar ratios. The QR-Atto-594 FRET pair showed a good spectral overlap and an acceptable $R_0$ of ~5.5 nm (ESI, Fig. S7†), ensuring that efficient FRET could take place over a reasonable $r$. Meanwhile, their emission spectra showed minimal overlap, allowing for easy separation of the donor–acceptor emissions without the need for spectral deconvolution. All the fluorescence spectra were recorded at $\lambda_{EX}$ = 450 nm, corresponding to the absorption minimum of Atto-594, to minimize the dye direct excitation background.[6] A progressively quenched QR fluorescence together with a concurrently enhanced Atto-594 FRET signal (at ~625 nm) were observed with an increase in the Affimer/QR ratio, which agreed well with the QR-sensitized Atto-594 dye FRET mechanism produced by QR-Affimer conjugation (ESI, Fig. S7C†). Fitting the FRET efficiency ($E$, determined from the QR donor quenching) dye/QR molar ratio relationship by a single QR donor in FRET interaction with an $N$ identical acceptor model,[14] $E = 1/[1 + (r/R_0)^6/N]$, gave an average FRET distance ($r$) of ~5.9 nm (ESI, Fig. S7D†). Given the rod shape rather than the spherical structure of the QR, and the inverse 6$^{th}$ power dependence of $E$ on $r$, the $r$ value derived from the FRET studies here would predominantly represent Affimers assembled on the QR next to the fluorescent CdSe core at the centre of the rod as revealed from EDX mapping (see the ESI, Fig. S1†). Those assembled at the ends of the rod would be too far away to produce strong FRET with the QR, and hence would contribute very little to the FRET results. Nonetheless, this result indicated the formation of a compact QR-Affimer structure, at least in the central rod region, making it well-suited for FRET based sensing applications.[12,13]

We subsequently employed the QR-Affimer (unlabeled) conjugate for detecting the target SUMO protein. Here QR-ZW each linked with 40 copies of unlabeled Affimer was mixed with an increasing amount of the target SUMO protein (Atto-594 labelled). Fig. 4 shows that, with an increase in the SUMO concentration, the QR fluorescence was greatly quenched while the Atto-594 FRET signal was enhanced simultaneously, consistent with the QR-sensitized Atto-594 FRET mechanism induced by Affimer–SUMO binding. A plot of the peak intensity ratio of Atto-594 to the QR, $I_{625}/I_{549}$, *versus* the SUMO concentration revealed a two stage linear relationship: a slow phase at lower concentrations (from 0.2 to 20 pM, fitting equation: $y = -1.95 + 0.12x$, $R^2 = 0.983$) and a rapid phase at higher concentrations (from 20 to 10 000 pM, $y = -2.37 + 0.41x$, $R^2 = 0.925$), respectively. The two stage FRET response described here appeared to resemble that of an earlier QD-FRET based DNA biosensor.[17b] The FRET ratio obtained with 5 pM protein was clearly above the limit of detection (indicated by the green dashed line, Fig. 4B) using the background + 3$\sigma$ criteria ($\sigma$: standard deviation).[30] This result suggested that the QR-Affimer sensor could ratiometrically

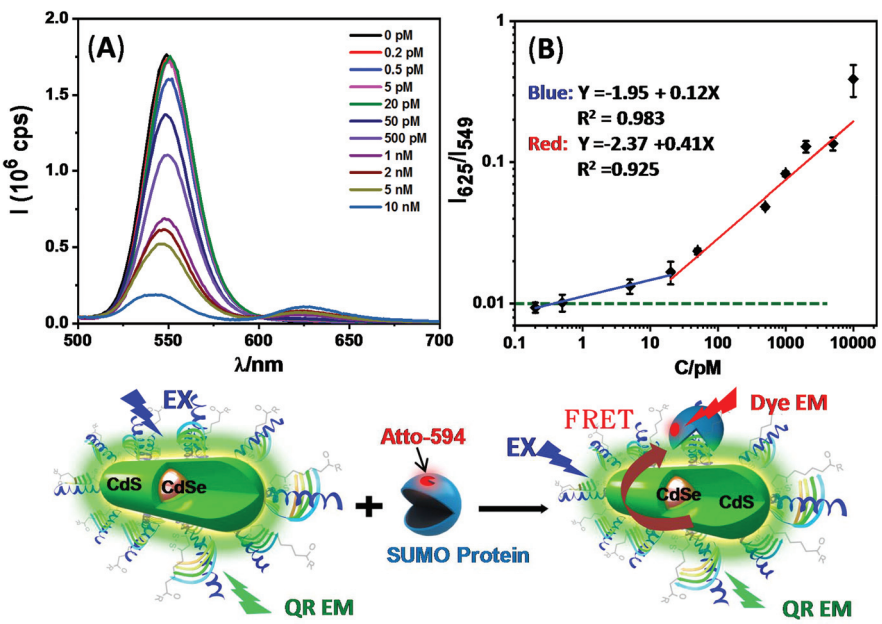


**Fig. 4** (A) Fluorescence spectra of the QR-Affimer conjugate (0.10 nM QR) after incubation with different amounts of Atto-594 labeled SUMO in PBS. (B) The relationship between the $I_{625}/I_{549}$ ratio *versus* the SUMO concentration (in the log–log plot). The data were best fitted in two linear functions, a slower increase between 0.2 and 20 pM ($R^2$ = 0.983) and a sharper increase at 20–10 000 pM ($R^2$ = 0.925). The dashed green line indicates the limit of detection based on the background + 3$\sigma$ criteria. The scheme beneath the figure showing the Affimer–SUMO protein binding induced FRET mechanism. Light symbols: blue (excitation light, EX); green (QR emission) and red (dye emission).

 

detect the target protein down to the low pM level. This sensitivity was comparable to some of the most sensitive QD-FRET based sensors for protein detection.[13]

We further investigated the potential of the QR-Affimer for detecting unlabeled proteins *via* a similar approach to that of the QD-Affimer reported previously.[12] Here we first conjugated each QR with 1 copy of the anti-SUMO Affimer (*via* $His_8$-tag self-assembly) and then blocked the QR surface with 40 copies of a control Affimer (also $His_8$-tagged) showing no binding affinity to the target SUMO protein.[23] An Atto-594 labeled SUMO protein (as the FRET reporter, 1 molar equivalent to the QR) was also added to develop the QR-Affimer sensing system.[12] Addition of unlabeled SUMO proteins would compete with the labelled SUMO binding to the QR-Affimer, reducing the FRET efficiency and giving rise to the QR fluorescence recovery in a dose dependent manner. A plot of the $I_{549}/I_{625}$ ratio *versus* the SUMO concentration revealed that the signal of 1 nM SUMO was clearly above the level of background + $3\sigma$, suggesting that it could detect unlabeled proteins down to the sub-nM level (see the ESI, Fig. S8†). This level of sensitivity was comparable to those of other sensitive QD-FRET sensors for the detection of unlabeled proteins.[13]

### 2.4. Preparation of QR-biotin for biosensing and cell imaging

Biotin-functionalized QRs were readily prepared by one-step cap-exchange using the mixed DHLA-$PEG_{600}$-biotin and DHLA-ZW ligands. Here we found that cap-exchange using a total LQMR of 1200 (1100 for DHLA-ZW and 100 for DHLA-$PEG_{600}$-biotin) could completely water-disperse the QR and form a stable dispersion (denoted as QR-$biotin_{100}$ hereafter). Moreover, by varying the DHLA-$PEG_{600}$-biotin to DHLA-ZW ligand ratio while keeping the total LQMR fixed at 1200 to perform cap-exchange, we were able to vary the QR surface biotin valency.[12] Using this method, QR-$biotin_{50}$ and QR-$biotin_{500}$ were also prepared for cancer cell imaging (see the next section, the detailed procedures are given in the ESI†).

QR-$biotin_{100}$ was first employed for neutravidin detection *via* the strong biotin–neutravidin binding ($K_d \sim 10^{-15}$ M).[31] As with the QR-ZW above, QR-$biotin_{100}$ was photon activated and then incubated with an increasing amount of neutravidin (Atto-594 labelled). A good positive linear response between the FRET ratio and the neutravidin concentration over 0–15 nM with a detection limit of ~0.2 nM was obtained (see the ESI, Fig. S9†). This sensor was highly specific: mixing Atto-594 labeled neutravidin (100 nM) with the control QR-ZW (1 nM, capped with the DHLA-ZW ligand only) gave no apparent quenching of the QR fluorescence. The FRET ratio of the control QR mixed with 100 nM neutravidin (corrected for dye direct excitation background) was 0.0042, <10% of that of 1 nM neutravidin binding to QR-$biotin_{100}$. Given a positive linear relationship between the FRET ratio and the amount of QR bound proteins,[4,6] this result indicated that the FRET signal obtained from the biotin–neutravidin binding was >1000 fold higher than that of non-specific adsorption, demonstrating an excellent sensing specificity.

Biotin is an important vitamin (known as vitamin H) and many cancer cells have shown to over-express biotin receptors, making it a useful ligand for cancer targeting.[32–34] Here bioti-

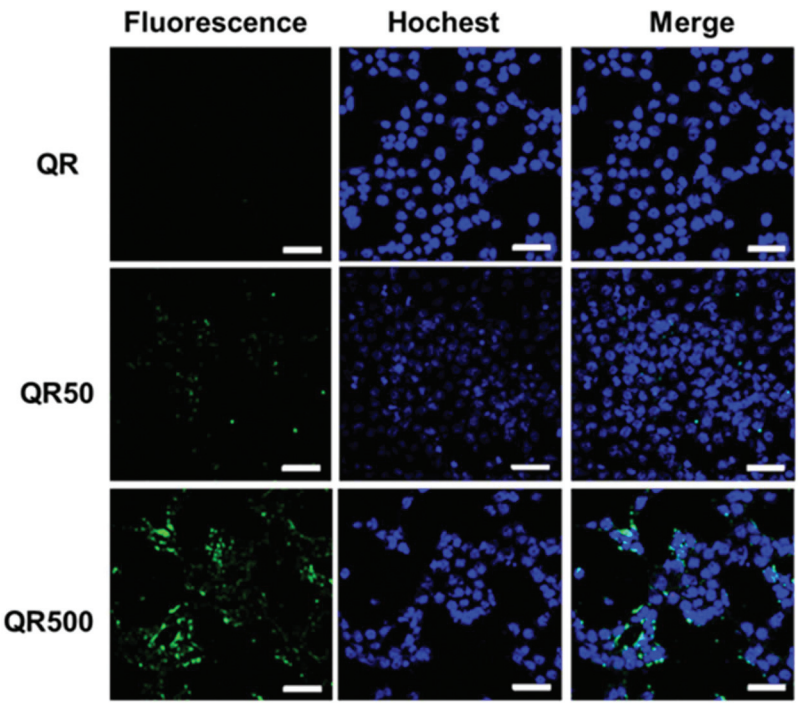


**Fig. 5** Confocal fluorescence images of 4T1 cells after 4 h treatment with 50 nM control QR-ZW (top, QR), QR-$biotin_{50}$ (middle, QR50) or QR-$biotin_{500}$ (bottom, QR500). From left to right, fluorescence images were recorded in the QR channel (green), Hochest channel (blue, staining nuclei) and the merged images of the QR/Hochest channels; scale bar = 50 μm.

nylated QRs were used to target the model 4T1 breast cancer cells *via* their surface over-expressed biotin receptors. The 4T1 cancer cells ($1.5 \times 10^5$ cells $mL^{-1}$) were incubated with the QR-ZW control, QR-biotin$_{50}$ or QR-biotin$_{500}$ (all at 50 nM final QR concentration) for 4 h, washed with phosphate-buffered saline, and then treated with Hochest 33342 for nuclei staining. The cells were then imaged by laser scanning confocal microscopy using 488 nm laser excitation and the QR emission at >525 nm was collected and exhibited a green colour. The 4T1 cells treated with the control QR-ZW displayed almost no green fluorescence, suggesting very little cell uptake (top panel, Fig. 5). In contrast, cells treated with the QR-biotins showed strong green fluorescence, and the cellular QR fluorescence appeared to be positively correlated to the QR surface biotin valency (Fig. 5). These results are consistent with the biotin receptor mediated cell uptake mechanism,[33,34] suggesting that the biotinylated QRs could be used for targeted fluorescence imaging of cancer cells.

## 3. Conclusions

To sum up, a highly efficient cap-exchange method was employed to water-disperse hydrophobic CdSe/CdS QRs to produce compact, biocompatible, but almost completely quenched QRs. Fortunately, the resulting QR fluorescence could be effectively regenerated *via* a novel photon activation method. Such fluorescence recovered QRs were successfully conjugated with His$_8$-tagged Affimers for the sensitive detection of 5 pM of a target protein. This cap-exchange method was successfully employed for the one-step preparation of biotin-functionalized QRs for the ratiometric detection of pM levels of neutravidin and also for specific imaging of cancer cells. Compared to the other methods reported in the literature, this method has the advantages of ease of operation (using air-stable ligands and rapid *in situ* reduction under ambient conditions), requirement of a minimal amount of ligands, and a simple light-activation process to regenerate QR fluorescence. The high brightness and compact structures of such photon regenerated QRs make them attractive fluorescent probes in broad biosensing and imaging applications, especially those relying on FRET-based readout strategies.

## Conflicts of interest

There are no conflicts of interest to declare.

## Acknowledgements

We thank the University of Leeds, the Wellcome Trust (Grant No: 097354/Z/11/Z), the Biotechnology and Biological Sciences Research Council (grant no: BB/R007829/1) and the EU Horizon 2020 *via* a Marie Sklodowska-Curie Fellowship (grant no: 797597) for funding this research.

## References

1 (*a*) M. Bruchez Jr., M. Moronne, P. Gin, S. Weiss and A. P. Alivisatos, *Science*, 1998, **281**, 2013–2016; (*b*) W. C. Chan and S. Nie, *Science*, 1998, **281**, 2016–2018.

2 (*a*) X. Michalet, F. Pinaud, L. Bentolila, J. Tsay, S. Doose, J. Li, G. Sundaresan, A. Wu, S. Gambhir and S. Weiss, *Science*, 2005, **307**, 538–544; (*b*) K. E. Sapsford, W. R. Algar, L. Berti, K. B. Gemmill, B. J. Casey, E. Oh, M. H. Stewart and I. L. Medintz, *Chem. Rev.*, 2013, **113**, 1904–2074; (*c*) K. D. Wegner and N. Hildebrandt, *Chem. Soc. Rev.*, 2015, **44**, 4792–4834; (*d*) I. L. Medintz and H. Mattoussi, *Phys. Chem. Chem. Phys.*, 2009, **11**, 17–45; (*e*) D. Zhou, *Biochem. Soc. Trans.*, 2012, **40**, 635–639.

3 (*a*) B. N. Giepmans, S. R. Adams, M. H. Ellisman and R. Y. Tsien, *Science*, 2006, **312**, 217–224; (*b*) D. R. Larson, W. R. Zipfel, R. M. Williams, S. W. Clark, M. P. Bruchez, F. W. Wise and W. W. Webb, *Science*, 2003, **300**, 1434–1436.

4 (*a*) I. L. Medintz, A. R. Clapp, F. M. Brunel, T. Tiefenbrunn, H. T. Uyeda, E. L. Chang, J. R. Deschamps, P. E. Dawson and H. Mattoussi, *Nat. Mater.*, 2006, **5**, 581–589; (*b*) I. L. Medintz, M. H. Stewart, S. A. Trammell, K. Susumu, J. B. Delehanty, B. C. Mei, J. S. Melinger, J. B. Blanco-Canosa, P. E. Dawson and H. Mattoussi, *Nat. Mater.*, 2010, **9**, 676–684; (*c*) C. Y. Zhang, H. C. Yeh, M. T. Kuroki and T. H. Wang, *Nat. Mater.*, 2005, **4**, 826–831.

5 (*a*) E. R. Smith, J. M. Luther and J. C. Johnson, *Nano Lett.*, 2011, **11**, 4923–4931; (*b*) W. R. Algar, M. G. Ancona, A. P. Malanoski, K. Susumu and I. L. Medintz, *ACS Nano*, 2012, **6**, 11044–11058.

6 (*a*) Y. Guo, C. Sakonsinsiri, I. Nehlmeier, M. A. Fascione, H. Y. Zhang, W. L. Wang, S. Pohlmann, W. B. Turnbull and D. J. Zhou, *Angew. Chem., Int. Ed.*, 2016, **55**, 4738–4742; (*b*) Y. Guo, I. Nehlmeier, E. Poole, C. Sakonsinsiri, N. Hondow, A. Brown, Q. Li, S. Li, J. Whitworth, Z. Li, A. Yu, R. Brydson, W. B. Turnbull, S. Pohlmann and D. Zhou, *J. Am. Chem. Soc.*, 2017, **139**, 11833–11844.

7 (*a*) L. S. Li, J. Hu, W. Yang and A. P. Alivisatos, *Nano Lett.*, 2001, **1**, 349–351; (*b*) A. Fu, W. Gu, B. Boussert, K. Koski, D. Gerion, L. Manna, M. Le Gros, C. A. Larabell and A. P. Alivisatos, *Nano Lett.*, 2007, **7**, 179–182.

8 (*a*) A. E. Albers, E. M. Chan, P. M. McBride, C. M. Ajo-Franklin, B. E. Cohen and B. A. Helms, *J. Am. Chem. Soc.*, 2012, **134**, 9565–9568; (*b*) S. Halivni, A. Sitt, I. Hadar and U. Banin, *ACS Nano*, 2012, **3**, 2758–2765; (*c*) K. Wu, L. J. Hill, J. Chen, J. R. McBridge, N. G. Pavlopolous, N. E. Richey, J. Pyun and T. Lian, *ACS Nano*, 2015, **9**, 4591–4599.

9 (*a*) R. Alam, D. M. Fontaine, B. R. Branchini and M. M. Maye, *Nano Lett.*, 2012, **12**, 3251–3256; (*b*) R. Alam, L. M. Karam, T. L. Doane, K. Coopersmith, D. M. Fontaine, B. R. Branchini and M. M. Maye, *ACS Nano*, 2016, **10**, 1969–1977.

10 (*a*) L. Manna, E. C. Scher, L.-S. Li and A. P. Alivisatos, *J. Am. Chem. Soc.*, 2002, **124**, 7136–7145; (*b*) J. J. Li, Y. A. Wang, W. Guo, J. C. Keay, T. D. Mishima, M. B. Johnson and X. Peng, *J. Am. Chem. Soc.*, 2003, **125**, 12567–12575.

11 D. Liu and P. T. Snee, *ACS Nano*, 2011, **5**, 546–550.
12 W. Wang, Y. Guo, C. Tiede, S. Chen, M. Kopytynski, Y. Kong, A. Kulak, D. Tomlinson, R. Chen, M. McPherson and D. Zhou, *ACS Appl. Mater. Interfaces*, 2017, **9**, 15232–15244.
13 (*a*) W. R. Algar, H. Kim, I. L. Medintz and N. Hildebrandt, *Coord. Chem. Rev.*, 2014, **263**, 65–85; (*b*) N. S. Hildebrandt, W. R. Algar, T. Pons, M. H. Stewart, E. Oh, K. Susumu, S. A. Díaz, J. B. Delehanty and I. L. Medintz, *Chem. Rev.*, 2017, **117**, 536–711.
14 (*a*) A. R. Clapp, I. L. Medintz, J. M. Mauro, B. R. Fisher, M. G. Bawendi and H. Mattoussi, *J. Am. Chem. Soc.*, 2004, **126**, 301–310; (*b*) E. R. Goldman, I. L. Medintz, J. L. Whitley, A. Hayhurst, A. R. Clapp, H. T. Uyeda, J. R. Deschamps, M. E. Lassman and H. Mattoussi, *J. Am. Chem. Soc.*, 2005, **127**, 6744–6751; (*c*) I. L. Medintz, J. Konnert, A. Clapp, I. Stanish, M. Twigg, H. Mattoussi, J. M. Mauro and J. Deschamps, *Proc. Natl. Acad. Sci. U. S. A.*, 2004, **101**, 9612–9617.
15 (*a*) K. Susumu, H. T. Uyeda, I. L. Medintz, T. Pons, J. B. Delehanty and H. Mattoussi, *J. Am. Chem. Soc.*, 2007, **129**, 13987–13996; (*b*) K. Susumu, B. C. Mei and H. Mattoussi, *Nat. Protoc.*, 2009, **4**, 424–436; (*c*) N. Zhan, G. Palui, H. Grise, H. Tang, I. Alabugin and H. Mattoussi, *ACS Appl. Mater. Interfaces*, 2013, **5**, 2861–2869.
16 M. Howarth, W. Liu, S. Puthenveetil, Y. Zheng, L. F. Marshall, M. M. Schmidt, K. D. Wittrup, M. G. Bawendi and A. Y. Ting, *Nat. Methods*, 2008, **5**, 397–399.
17 (*a*) D. Zhou, Y. Li, E. A. H. Hall, C. Abell and D. Klenerman, *Nanoscale*, 2011, **3**, 201–211; (*b*) H. Zhang, G. Feng, Y. Guo and D. Zhou, *Nanoscale*, 2013, **5**, 10307–10315; (*c*) D. Zhou, L. Ying, X. Hong, E. A. Hall, C. Abell and D. Klenerman, *Langmuir*, 2008, **24**, 1659–1664.
18 (*a*) W. Liu, M. Howarth, A. B. Greytak, Y. Zheng, D. G. Nocera, A. Y. Ting and M. Bawendi, *J. Am. Chem. Soc.*, 2008, **130**, 1274–1284; (*b*) E. Muro, T. Pons, N. Lequeux, A. Fragola, N. Sanson, Z. Lenkei and B. Dubertret, *J. Am. Chem. Soc.*, 2010, **132**, 4556–4557.
19 L. Ma, C. L. Tu, P. Le, S. Chitoor, S. J. Lim, M. U. Zahid, K. W. Teng, P. H. Ge, P. R. Selvin and A. M. Smith, *J. Am. Chem. Soc.*, 2016, **138**, 3382–3394.
20 W. H. Liu, A. B. Greytak, J. Lee, C. R. Wong, J. Park, L. F. Marshall, W. Jiang, P. N. Curtin, A. Y. Ting, D. G. Nocera, D. Fukumura, R. K. Jain and M. G. Bawendi, *J. Am. Chem. Soc.*, 2010, **132**, 472–483.
21 W. Wang, X. Ji, A. Kapur, C. Zhang and H. Mattoussi, *J. Am. Chem. Soc.*, 2015, **137**, 14158–14172.
22 (*a*) Y. Chen, J. Vela, H. Htoon, J. L. Casson, D. J. Werder, D. A. Bussian, V. I. Klimov and J. A. Hollingsworth, *J. Am. Chem. Soc.*, 2008, **130**, 5026–5027; (*b*) J. Zhou, M. Zhu, R. Meng, H. Qin and X. Peng, *J. Am. Chem. Soc.*, 2017, **139**, 16556–16567; (*c*) Y. Shi, R. Tan, M. Y. Gee and A. B. Greytak, *ACS Nano*, 2015, **9**, 3345–3359.
23 (*a*) C. Tiede, A. A. Tang, S. E. Deacon, U. Mandal, J. E. Nettleship, R. L. Owen, S. E. George, D. J. Harrison, R. J. Owens and D. C. Tomlinson, *Protein Eng., Des. Sel.*, 2014, **27**, 145–155; (*b*) C. Tiede, R. Bedford, S. J. Heseltine, G. Smith, I. Wijetunga, R. Ross, D. AlQallaf, A. P. Roberts, A. Balls, A. Curd, R. E. Hughes, H. Martin, S. R. Needham, L. C. Zanetti-Domingues, Y. Sadigh, T. P. Peacock, A. A. Tang, N. Gibson, H. Kyle, G. W. Platt, N. Ingram, T. Taylor, L. P. Coletta, I. Manfield, M. Knowles, S. Bell, F. Esteves, A. Maqbool, R. K. Prasad, M. Drinkhill, R. S. Bon, V. Patel, S. A. Goodchild, M. Martin-Fernandez, R. J. Owens, J. E. Nettleship, M. E. Webb, M. Harrison, J. D. Lippiat, S. Ponnambalam, M. Peckham, A. Smith, P. K. Ferrigno, M. Johnson, M. J. McPherson and D. C. Tomlinson, *eLife*, 2017, **6**, e24903.
24 J. A. Burns, J. C. Butler, J. Moran and G. M. Whiteside, *J. Org. Chem.*, 1991, **56**, 2648–2650.
25 (*a*) J. A. Barltrop, P. M. Hayes and M. Calvin, *J. Am. Chem. Soc.*, 1954, **76**, 4348–4367; (*b*) G. Palui, T. Avellini, N. Zhan, F. Pan, D. Gray, I. Alabugin and H. Mattoussi, *J. Am. Chem. Soc.*, 2012, **134**, 16370–16378.
26 E. Petryayeva, W. R. Algar and I. L. Medintz, *Appl. Spectrosc.*, 2013, **67**, 215–252.
27 (*a*) D. Peer, J. M. Karp, S. Hong, O. C. Farokhzad, R. Margalit and R. Langer, *Nat. Nanotechnol.*, 2007, **2**, 751–760; (*b*) H. S. Choi, W. Liu, P. Misra, E. Tanaka, J. P. Zimmer, B. I. Ipe, M. G. Bawendi and J. V. Frangioni, *Nat. Biotechnol.*, 2007, **25**, 1165–1170.
28 Y. Zhang, S. W. Yuan, R. Lu and A. C. Yu, *J. Phys. Chem. B*, 2013, **117**, 7308–7316.
29 (*a*) V. I. Klimov, *Annu. Rev. Phys. Chem.*, 2007, **58**, 635–673; (*b*) V. I. Klimov and D. W. McBranch, *Phys. Rev. B: Condens. Matter Mater. Phys.*, 1990, **60**, 13740–13749.
30 (*a*) D. M. Rissin, C. W. Kan, T. G. Campbell, S. C. Howes, D. R. Fournier, L. Song, T. Piech, P. P. Patel, L. Chang and A. J. Rivnak, *Nat. Biotechnol.*, 2010, **28**, 595–599; (*b*) L. D. S. Lapitan Jr., Y. Xu, Y. Guo and D. Zhou, *Nanoscale*, 2019, **11**, 1195–1204.
31 Thermo Scientific Pierce Protein Research Products 2009 Catalog. https://thermofisher.portica.de/system/includes/download.php?f=1033.
32 N. Nateghian, N. Goodarzi, M. Amini, F. Atyabi, M. R. Khorramizadeh and R. Dinarvand, *Chem. Biol. Drug Des.*, 2016, **87**, 69–82.
33 (*a*) Y. Singh, R. Durga, K. K. Viswanadham, A. J. Kumar, J. G. Meher, K. Raval, S. Jaiswal, J. Dewangan, H. K. Bora, S. K. Rath, J. Lal and D. P. Mishra, *Mol. Pharm.*, 2017, **14**, 2749–2765; (*b*) S. Park, E. Kim, W. Y. Kim, C. Kang and J. S. Kim, *Chem. Commun.*, 2015, **51**, 9343–9345.
34 (*a*) L. Lv, Y. Guo, Y. Shen, J. Liu, W. Zhang, D. Zhou and S. Guo, *Adv. Healthcare Mater.*, 2015, **4**, 1496–1501; (*b*) J. Wang, F. Wang, F. Li, W. Zhang, Y. Shen, D. Zhou and S. Guo, *J. Mater. Chem. B*, 2016, **4**, 2954–2962.